Analysis of Scintillation Effects in Terahertz Band Satellite Communications for 6G and Beyond

Sergi Aliaga
Northeastern University
Boston, MA, United States
aliaga.s@northeastern.edu

Vitaly Petrov
KTH Royal Institute of Technology
Stockholm, Sweeden
vitalyp@kth.se

Tejinder Singh
Dell Technologies
Ottawa, Canada
singh.tejinder@dell.com

Mohammad Alavirad
Dell Technologies
Ottawa, Country
mohammad.alavirad@dell.com

Morris Repeta
Dell Technologies
Ottawa, Canada
morris.repeta@dell.com

Michael Healy
Dell Technologies
Hopkinton, MA, United States
mike.healy@dell.com

Josep M. Jornet
Northeastern University
Boston, MA, United States
j.jornet@northeastern.edu

2025 IEEE 22nd Consumer Communications & Networking Conference (CCNC) | 979-8-3315-0805-0/25/$31.00 ©2025 IEEE | DOI: 10.1109/CCNC54725.2025.10976007

***Abstract*—Scintillation due to atmospheric turbulence is one of the effects challenging the reuse of extremely wideband and high-rate optical satellite-to-satellite communication systems for satellite-to-Earth and Earth-to-satellite transmissions. In this article, we study the possibility of utilizing links in the terahertz (THz) frequency bands for these uplink and downlink transmissions instead. Built upon the physics-based model, originally developed for optical wave propagation, we present a mathematical framework for the THz signal scintillation to analyze atmospheric turbulence's impact on ground-satellite and airplane-satellite connections. Our results indicate that, while the scintillation still significantly impacts the power of the received THz signal (especially at lower elevation angles and under specific weather conditions), the effect is drastically less profound than the extreme losses the optical link will experience in the same weather conditions. We further explore a notable asymmetry of up to 10 dB between uplink and downlink losses. Finally, we illustrate that, even at relatively low airplane altitudes, the airplane-to-satellite link is much less affected than the Earth-to-satellite link, making THz communications a promising candidate technology for future high-rate airplane connectivity systems as a part of 6G and beyond.**

I. Introduction

Facilitating ultra-broadband communication between Earth and space essential for integrating high-speed satellite communications into the sixth-generation (6G) cellular network landscape. Specifically, providing global high-rate connectivity via massive constellations of Low-Earth Orbit (LEO) satellites is a crucial facilitator for high-speed Internet access around the world [1]. Despite the large data rates achievable in inter-satellite communication links thanks to favorable propagation conditions [2], [3], one of the bottlenecks is the links between Terrestrial and Non-Terrestrial Network (NTN) segments [4].

Existing solutions by Apple-Globalstar, Qualcomm-Iridium, and SpaceX, are still limited to relatively low data rates: SOS messages and LTE-level Internet on the move [5], or a few (hundreds of) Mbps data connectivity maximum if using a large-scale antenna [6]. The latter is often sufficient for a single household, but not enough to provide high-rate Internet access to a 6G cell covering a remote area on the ground or to each of the 300-plus airplane passengers during a long-haul flight.

In theory, the rate over ground-satellite and airplane-satellite links can be notably boosted by exploiting already established broadband direct satellite-to-satellite cross-link Free-Space Optics (FSO) communication solutions. However, in practice, FSO ground-to-satellite links get severely degraded even in clear-sky conditions. On top of the substantial spreading loss at optical frequencies, *scintillation* – the random fluctuations of a propagating Electromagnetic (EM) wave due to wavefront deformation caused by inhomogeneities in the propagation medium – is an issue when communicating with the satellites through the atmosphere, as reported by Kaushal et al. [7].

Many studies exploring this effect further are based on *optical* scintillation models developed from established air turbulence theory [8], including Andrews et al. [9], which explored the changes in the laser signal when affected by turbulence. Furthermore, Rhui-Zong et al. [10] later simplified the results from [8] for *optical* plane and spherical waves, while Ashraf et al. [11] characterized the received power under scintillation for different *optical* wavelengths. However, these comprehensive FSO-related findings cannot be applied as is to THz due to the non-linear dependency present between the signal frequency and the additional turbulence-induced loss in the signal when propagating through a non-homogeneous atmosphere [9].

On the other side, the overwhelming majority of modern THz-specific models, including but not limited to [12]–[18] (among many others) focus on other impairments at THz frequencies, such as spreading loss, molecular absorption loss, scattering loss, and scattering noise, *while not considering the turbulence-induced scintillation effects* – the focus of this work. Recently, one of the initial attempts to characterize turbulence-induced losses at THz was made in [19] for THz drone-to-drone links at a given *fixed* altitude. Hence, the model does not apply to ground-satellite and airplane-satellite THz links over a range of altitudes with notably different turbulence levels [9], thus giving the motivation for the present study of this phenomenon.

The main contributions of this work are:

- We present a constructive approach to quantify the scintillation-induced losses in THz links between a ground station or an airplane and a THz satellite. *Notably, the developed model highlights a non-conventional asymmetry between the losses in uplink and downlink THz links.*

- We then utilize this approach for a comprehensive numerical study to assess the impact of scintillation losses on ground-satellite and airplane-satellite THz links.

II. System Model

The system model for this study comprises a satellite orbiting at altitude H above sea level, a ground station (GS) at altitude $h_{0,\text{GS}}$, and an airplane at altitude $h_{0,\text{A}}$, as in Fig. 1. Focusing on carefully modeling the scintillation-related effects, we disregard molecular scattering and absorption. Scintillation, the primary physical channel impairment, stems from turbulent airflow in the atmospheric layers between the satellite, the GS, and the airplane. This turbulence induces random temperature fluctuations along the propagation path, resulting in a variable refraction index. Consequently, the propagation space between the satellite and the Earth becomes an inhomogeneous medium.

The next section summarizes a constructive approach to model the turbulence-caused fading in THz ground-satellite and airplane-satellite links, while additional clarifications on the theory behind this presented approach are in Appendix A.

III. Scintillation Model for THz Satellite Links

A. Atmospheric turbulence and refractive index structure

The strength of atmospheric turbulence is typically characterized by quantifying the strength of the fluctuations in the refractive index, $n(\mathbf{r},t)$, denoted as *the refractive index structure constant (RISC)*, $C_n^2(h)$, measured in $\text{m}^{-2/3}$, where h denotes the altitude [20]. Even at sea level ($h=0$), the exact value of $C_n^2(0)$ may vary notably depending on the current atmospheric conditions (primarily wind speed) and typically lies within the range from $10^{-17}\text{m}^{-2/3}$ and $10^{-13}\text{m}^{-2/3}$ [9].

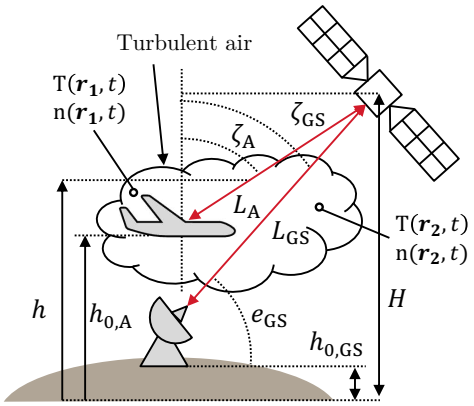

Fig. 1: Modeling ground-satellite and airplane-satellite THz communications across atmospheric turbulence.

At ground level, the statistics of $C_n^2(h)$ can be measured for a given area over long periods, providing reliable data. In contrast, the setup complexity increases notably for slant paths (ground- and airplane-satellite links). There, the turbulent wind speed may vary considerably with altitude and, therefore, the altitude dependency of the RISC needs to be captured. It is theoretically possible to conduct an extensive measurement campaign at all the altitudes of interest over a given location (e.g., an airport or a candidate location for a ground satellite station). However, from a practical point of view, such an approach often faces severe engineering challenges and associated costs. Therefore, built upon modern atmospheric studies, analytical models to approximate $C_n^2(h)$ for a given altitude h and a defined $C_n^2(0)$ at sea level are utilized.

A widely accepted RISC model, derived from measurements at optical frequencies, is the Hufnagel-Valley (H-V) model:

$$C_{n,\text{FSO}}^2(h) = 0.00594(w/27)^2(10^{-5}h)^{10}\exp(-h/1000) + 2.7\times10^{-16}\exp(-h/1500) + C_n^2(0)\exp(h/100), \quad (1)$$

first introduced by R. E. Hufnagel [21], and later modified by G. C. Valley [22]. In (1), w stands for the root mean square (rms) windspeed along the propagation path.

The lack of experimental data in the THz band has prevented the appearance of similar measurement-based RISC models at such frequencies. However, as indicated in [19], a RISC model at THz frequencies can be derived using the relation between C_n^2 and the temperature, $T(\mathbf{r},t)$, structure constant, C_T^2, given by $C_T^2 = C_n^2\left(\partial n(T)/\partial T\right)^{-2}$. Given that temperature is not a frequency-dependent quantity, its structure parameter is also frequency-invariant, and the RISC at the two different bands can therefore be related as:

$$C_{n,\text{THz}}^2(h) = C_{n,\text{FSO}}^2(h)\left(\frac{\partial n_{\text{THz}}(T)}{\partial T}\right)^2 \Big/ \left(\frac{\partial n_{\text{FSO}}(T)}{\partial T}\right)^2. \quad (2)$$

The expressions for the relation between the index of refraction at THz and optical frequencies with temperature are [23]:

$$n_{\text{THz}}(T) = 1 + 7.76\times10^{-6}\left(P_a/T + 4810P_v/T^2\right) \quad (3)$$

$$n_{\text{FSO}}(T) = 1 + 7.76\times10^{-6}P_a/T, \quad (4)$$

where P_a and P_v are the atmospheric and water vapor pressures in kilopascal, respectively. Replacing (3) and (4) in (2) results in:

$$C_{n,\text{THz}}^2(h) = C_{n,\text{FSO}}^2(h)\left(1 + 9620P_v/(P_aT)\right)^2 \approx C_{n,\text{FSO}}^2(h), \quad (5)$$

where the fraction P_v/P_a represents the volumetric concentration of water vapor in the atmosphere, according to Dalton's Law of partial pressures in gaseous mixtures. Given the upper value of 4% for this volumetric concentration [24], only reached in tropical climates, the approximation in (5) holds, and thus the H-V model is valid at THz frequencies as well.

B. Scintillation index and irradiance distribution

To characterize the scintillation on long-range THz links, we first convert the obtained $C_{n,\text{THz}}^2(h)$ into the scintillation index σ_I^2 (normalized irradiance variance caused by scintillation) of a plane wave propagating through a turbulent media with varying RISC. We particularly reference a simpler model and analysis in [9] for FSO and constant latitude of the propagation path. Among other findings, the study in [9] specifically reveals that the scintillation is a fast-fading channel impairment, affecting the transmitted signal on small time and distance scales while not affecting the mean received signal strength (large scale).

Extending the model for σ_I^2 [9] to the slant path case ($h_{\text{Start}} \neq h_{\text{End}}$), we derive the following two expressions for the scintillation index of a wave traveling in uplink (UL, e.g.,

ground-to-satellite) and downlink (DL, e.g., satellite-to-ground) directions:

$$\sigma^2_{I,\mathrm{UL}}(f,\zeta,h_0,H) = M(f,\zeta)\int_{h_0}^{H} C_n^2(h)(H-h)^{5/6}\mathrm{d}h \quad (6)$$

$$\sigma^2_{I,\mathrm{DL}}(f,\zeta,h_0,H) = M(f,\zeta)\int_{h_0}^{H} C_n^2(h)(h-h_0)^{5/6}\mathrm{d}h \quad (7)$$

$$M(f,\zeta) = 2.25\left(\frac{2\pi f}{c}\right)^{7/6}\sec^{11/6}(\zeta), \quad (8)$$

where $\sigma^2_{I,\mathrm{UL}}(h_0,H)$ and $\sigma^2_{I,\mathrm{DL}}(h_0,H)$ are the corresponding UL and DL scintilation indexes, f stands for the frequency of the transmitted signal, c is the speed of light in the atmosphere, h_0 is the altitudes of the ground station ($h_0 = h_{0,\mathrm{GS}}$) or the airplane ($h_0 = h_{0,\mathrm{A}}$), depending on the modeled link, and H is the satellite altitude. In these equations, $C_n^2(h)$ is the altitude-dependent RISC following (1), $\sec(\zeta)$ stands for the secant of angle ζ, and ζ corresponds to the zenith angle from the ground station or the airplane to the satellite illustrated in Fig. 1 (either $\zeta = \zeta_{\mathrm{GS}}$ or $\zeta = \zeta_{\mathrm{A}}$ depending on the modeled link), complementary to the corresponding elevation angle (e.g., $\zeta_{\mathrm{GS}} = \pi/2 - e_{\mathrm{GS}}$ for the ground-satellite link, see Fig. 1).

Expressions in (6) and (7) are similar except for the balancing factors inside the integral giving a notably larger weight to the turbulence closer to the transmitter. *Hence, we conclude that the scintillation introduces important asymmetry between the uplink and downlink to the satellite*, as detailed in Sec. IV.

C. Field irradiance and fading

There has been considerable effort in obtaining a general probability density function (PDF) for the field irradiance at the receiver from its derived statistical moments, including σ_I^2 [9]. Although a myriad of statistical models have been presented to date, in this work, we adopt the model featuring a good fit with experimental data under all turbulence conditions, following the Gamma-Gamma distribution [25]:

$$f_I(I) = \frac{2(\alpha\beta)^{\frac{\alpha+\beta}{2}}}{\Gamma(\alpha)\Gamma(\beta)} I^{\frac{\alpha+\beta}{2}-1} K_{\alpha-\beta}(2\sqrt{\alpha\beta I}), \quad (9)$$

$$\alpha = \left\{\exp\left[0.49\sigma_I^2/\left(1+1.11\sigma_I^{12/5}\right)^{7/6}\right]-1\right\}^{-1}, \quad (10)$$

$$\beta = \left\{\exp\left[0.51\sigma_I^2/\left(1+0.69\sigma_I^{12/5}\right)^{5/6}\right]-1\right\}^{-1}, \quad (11)$$

where $\Gamma(\cdot)$ stands for the Gamma function, $K_p(z)$ is the modified Bessel function of the second kind, while α and β are shape parameters that depend on the scintillation conditions, i.e., σ_I^2. Additionally, the field irradiance I in (9) has been normalized such that $\langle I\rangle = 1$, where the $\langle\cdot\rangle$ operator denotes the *ensemble average* or *expected value*.

We utilize (9) in our analysis by parameterizing α and β in this PDF model with our derived expressions for UL and DL THz links: $\sigma_I = \sigma^2_{I,\mathrm{UL}}(f,\zeta,h_0,H)$ or $\sigma_I = \sigma^2_{I,\mathrm{DL}}(f,\zeta,h_0,H)$.

Finally, the fading statistics of the received signal can be directly derived from the statistics of the received field irradiance, given the scenario geometry. For propagating distances in the scale of satellite communication scenarios (> 100 km), both

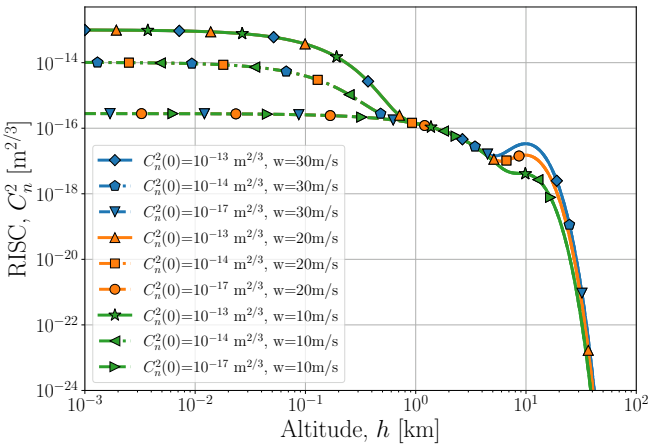

Fig. 2: Hufnagel-Valley model of atmospheric turbulence.

GS and satellite can be modeled as point receivers [26]. Hence, the received signal power is proportional to the field irradiance at the receiver, with the receiving effective antenna aperture acting as the proportionality constant. With these assumptions, the probability of fade can be directly computed from the cumulative distribution function (CDF) of the irradiance as:

$$P(F \geq F_T) = P(I \leq I_T), \quad (12)$$

where $F_T = -10\log_{10}(I_T)$ is the fading threshold given a certain normalized irradiance threshold, I_T.

IV. Results

We numerically elaborate on the developed model for THz ground-to-satellite and airplane-to-satellite links in this section. Whenever applicable, we also contrast the results with those achievable for FSO (optical) links.

We start with Fig. 2 presenting the $C_n^2(h)$ values from (1) as a function of the altitude h for different combinations of sea-level $C_n^2(0)$ and rms windspeed w values. Two important observations are made from this figure: (i) turbulence conditions in the atmosphere are only noticeable in the first $\simeq 20$ km above

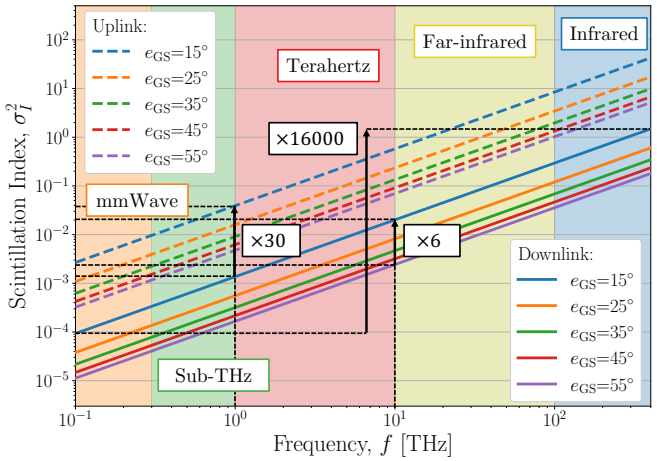

Fig. 3: Scintillation index at different frequencies under identical ground turbulence conditions.

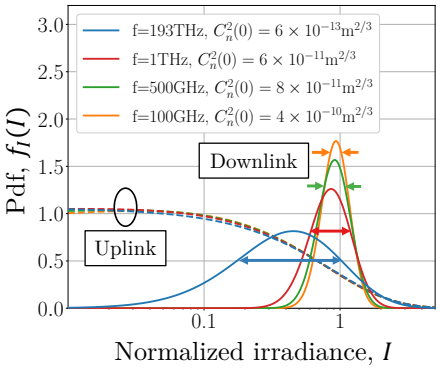

Fig. 4: Normalized irradiance PDF at the ground station.

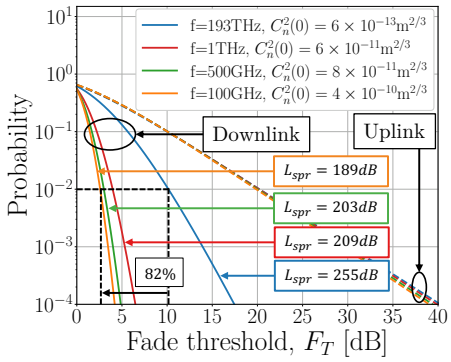

Fig. 5: Scintillation fade probability at the ground station.

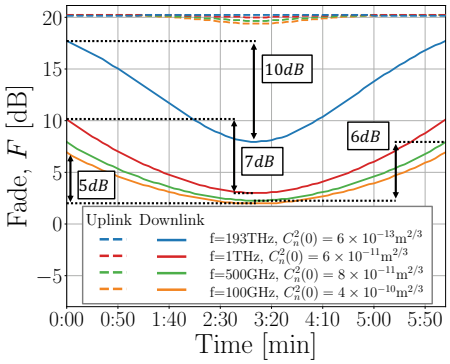

Fig. 6: Scintillation fading with a 1% probability during a satellite contact.

the ground, and (ii) the dependency on $C_n^2(0)$ largely dominates the RISC values at low altitudes, whereas the dependency on w dominates the RISC values at the highest altitudes. These observations are useful for a better understanding of the results and trends discussed below.

Studying how the main system variables impact the scintillation present in the received signal for a given set of turbulence conditions, Fig. 3 depicts the scintillation index, σ_I, for UL and DL links following (6) and (7), as a function of frequency, f, and for different elevation angles e_{GS}. The satellite altitude is set to $H = 500$ km and the ground turbulence conditions are set to $C_n^2(0) = 4 \times 10^{-15}$ m$^{2/3}$, and $w = 20$ m/s. The integrals in (6) and (7) are evaluated numerically.

Most notably, scintillation varies significantly across frequency bands, with the index increasing log-linearly and showing four orders of magnitude difference between millimeter-wave and infrared bands, highlighting the impact of frequency on satellite link scintillation. Additionally, there's a notable asymmetry between uplink (UL) and downlink (DL) transmissions, with UL experiencing scintillation an order of magnitude greater due to the larger impact of ground-level turbulence, as explained by the H-V model's findings on atmospheric turbulence reduction with altitude. Furthermore, scintillation is significantly affected by the elevation angle, with low angles suffering more due to longer signal paths through varying atmospheric conditions, intensifying the scintillation effect.

Fig. 4 introduces the PDF of normalized irradiance at an $e_{GS} = 45°$ elevation angle for a ground station, highlighting the differences in field irradiance distributions between uplink and downlink due to turbulence. In the downlink, the probability density function narrows with decreasing frequency, approaching a delta function, and indicating minimal fast fading and a more stable received signal strength at frequencies below 100 GHz. It is crucial to acknowledge the variations in the ground RISC across frequencies, with extreme $C_n^2(0)$ values outside the optical range (e.g., 4×10^{-10} at 100 GHz). Given typical values range from 10^{-17} m$^{2/3}$ to 10^{-13} m$^{2/3}$, the considered values are highly improbable and only conceivable under catastrophic weather conditions.

Fig 5 illustrates fade probabilities across different frequencies, further highlighting that in the downlink, fades vary significantly with frequency, showcasing up to 82% lower fade with 1% probability of occurrence at lower frequencies compared to FSO technology. In the uplink, ground turbulence is substantial enough to obscure any frequency-based differences in fade. Despite the presence of scintillation fading, it is markedly less impactful than spreading losses, included in the figure for reference, and indicating that other channel impairments play a more significant role in signal degradation.

Fig. 6, generated using our custom satellite communications framework introduced in [3], showcases fade versus time during a 6 min and 10 s satellite contact with a GS in Boston, (42.35545, −71.06547), revealing the dynamics of scintillation on the satellite access link. The framework, developed in Python 3.8, simulates the geometry, mobility, and orbital dynamics of satellites, as well as the characteristics of LEO mmWave and THz wireless directional links. The results indicate that scintillation fading is minimal at the highest elevation point of the satellite pass, while the start and end of the pass, which require pointing at lower elevation angles, experience the highest scintillation losses, up to 10 dB. Notably, the scintillation loss difference between the highest elevation and the pass's extremities is less pronounced at lower frequencies, with a mere 5 dB variation observed at 100 GHz.

Fig. 7 explores the effects of atmospheric turbulence on scintillation fading for FSO and THz satellite links, comparing ground-based FSO links with those on airplanes at various altitudes. The analysis, considering a 30° elevation angle, a $C_n^2(0) = 10^{-11}$ of 10^{-11}, and rms windspeed $w = 20$ m/s., shows a significant improvement in the performance of airplane-satellite FSO links with increasing altitude. Specifically, there is up to a 98% reduction in scintillation fade at a 1 % probability for downlink scenarios at an altitude of 6 km, making the performance of airborne FSO links nearly comparable to ground-based THz links. This improvement is even more pronounced in the uplink scenario, with a 91% reduction in scintillation fade at a 1% probability. These findings suggest that airplane FSO links can be significantly less affected compared to ground-to-satellite FSO links, and indicate that the choice between THz and FSO technologies for the satellite access link should be based on the specific scenario and turbulence conditions, highlighting their potential

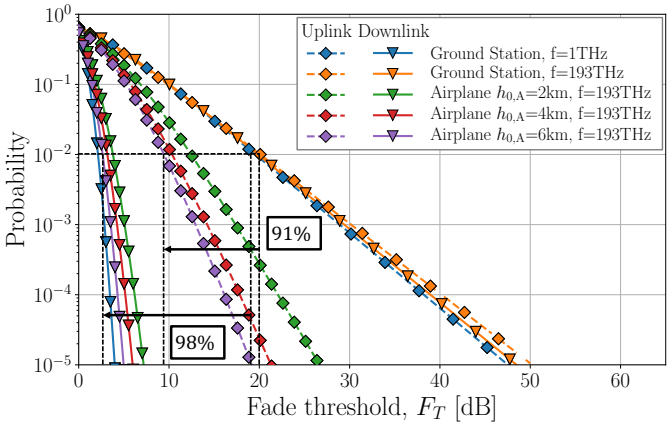

Fig. 7: Comparison of scintillation fade probability at different airplane altitudes with ground-satellite THz and FSO links.

complementary roles.

V. Conclusions

This article provides an important building block (scintillation loss model over links through various altitudes) to be integrated into next-generation THz channel models for satellite communications that already account for spreading, absorption, and scattering losses. Our numerical study illustrates that these additional scintillation-related losses may vary between 2 dB and 20 dB for THz, and hence should not be ignored. Further, the presented comparison of the turbulence-induced losses in THz and FSO ground-satellite communications demonstrates a notable advantage of the former as a candidate choice for next-generation high-rate ground-satellite communication systems.

Importantly, it is numerically illustrated that THz satellite links are of particular interest for airplanes, as the airplane-satellite links feature not only, as expected, lower spreading and absorption losses [14], but also notably less profound scintillation losses, as revealed in the present study. Last but not least, an important novel asymmetry is revealed between the losses over UL (e.g., ground-to-satellite and airplane-to-satellite) and DL (e.g., satellite-to-ground and satellite-to-airplane) that should be accounted for in the design and analysis of future THz satellite communications for 6G and beyond.

Appendix A
Turbulence and Scintillation Theory

A. Time-averaged Effect of Turbulence

In classic turbulence theory, the temperature, $T(x,y,z,t)$, and index of refraction, $n(x,y,z,t)$, in a turbulent medium are modeled as random scalar fields. Taylor's frozen turbulence hypothesis [27] allows for the complete characterization of these fields through spatial analysis alone, $n(x,y,z,t) \equiv n(x,y,z) \equiv n(\mathbf{R})$, given the characteristics of turbulent airflow motion in the atmosphere. A random field, $n(\mathbf{R})$, can be statistically characterized by the Fourier pair formed by its three-dimensional autocovariance function, $B_n(\mathbf{R})$, and spatial spectrum, $\Phi_n(\mathbf{k})$, where $\mathbf{k}$ is the *spatial frequency*. The spatial spectrum of homogeneous index of refraction fluctuations is often modeled via the *Kolmogorov power-law spectrum* [8]:

$$\Phi_n(k) = 0.0033 C_n^2 k^{-11/3}. \tag{13}$$

B. Scintillation of the THz EM wave

Scintillation, the effect of atmospheric turbulence on EM wave propagation, is modeled as random complex perturbations of the transmitted field. If $U_0(\mathbf{r},z)$ represents the unperturbed field amplitude of a propagating wave in cylindrical coordinates, $u(\mathbf{r},z,t) = U_0(\mathbf{r},z)e^{-\omega t}$, the resulting field amplitude through turbulence, $U(\mathbf{r},z)$, is:

$$U(\mathbf{r},z) = U_0(\mathbf{r},z)\exp[\psi_1(\mathbf{r},z) + \psi_2(\mathbf{r},z) + ...], \tag{14}$$

where $\psi_i(\mathbf{r},z)$ are the complex perturbations, the z-axis is defined by the direction of propagation, and $\mathbf{r} \equiv (x,y)$. The expression in (14) is known as the *Rytov approximation* to solve the *stochastic Helmholtz equation*, which is derived from the original wave equation when considering an inhomogeneous medium, i.e., $n = n(\mathbf{R})$:

$$\nabla^2 U(\mathbf{R}) + k^2 n^2(\mathbf{R}) U(\mathbf{R}) = 0. \tag{15}$$

Under these assumptions, the different statistical moments of $U(\mathbf{r},z)$ can be derived to develop a channel model of a wireless communications system operating under turbulence. The second-order and fourth-order moments, also known as *mutual coherence function* and *cross-coherence function*, provide the essential information to characterize the received field irradiance, defined as its squared amplitude, $I(\mathbf{r},z) \equiv |U(\mathbf{r},z)|^2$. In particular, the average and variance of the field irradiance are determined, respectively, by:

$$\langle I(\mathbf{r},z)\rangle = \langle U(\mathbf{r},z)U^*(\mathbf{r},z)\rangle \tag{16}$$

$$\sigma_I^2(\mathbf{r},z) = \frac{\langle I^2(\mathbf{r},z)\rangle}{\langle I(\mathbf{r},z)\rangle^2} - 1 = \langle |U(\mathbf{r},z)|^2\rangle, \tag{17}$$

where $\langle\cdot\rangle$ denotes the ensemble average. The irradiance variance, σ_I^2, is known as the *scintillation index*.

Using (16) under the assumption that the index of refraction follows Kolmogorov's spectrum implies that, on average, the turbulence doesn't change the mean irradiance of the wave.

C. Gamma-Gamma distribution

The Gamma-Gamma distribution in (9) is derived from modeling the square of the first two perturbations in (14), $\exp[\psi_i(\mathbf{r},z)], \forall i \in [1,2]$, as Gamma-distributed modulating variables. In this way, large-scale perturbations ($i=1$) and small-scale perturbations ($i=2$) are modeled as iid random variables, given the dynamics of atmospheric turbulent air masses.

Acknowledgment

This work has been supported in part by the projects CNS-1955004 and CNS-2011411 by the National Science Foundation (NSF), as well as by the U.S. Air Force FA9550-23-1-0254. This project was also supported in part by a fellowship from "la Caixa" foundation (ID 100010434, LCF/BQ/AA20/11820041). V. Petrov acknowledges the support from Digital Futures and Grant 2022-04222 from the Swedish Research Council (VR).

REFERENCES

[1] 3GPP, "Study on New Radio (NR) to support non-terrestrial networks," 3GPP TR 38.811 V15.4.0, Oct 2020.

[2] J. M. Jornet, V. Petrov, H. Wang, Z. Popović, D. Shakya, J. V. Siles, and T. S. Rappaport, "The evolution of applications, hardware design, and channel modeling for Terahertz (THz) band communications and sensing: Ready for 6G?" *Proceedings of the IEEE*, pp. 1–32, July 2024.

[3] S. Aliaga, V. Petrov, and J. M. Jornet, "Modeling interference from millimeter wave and Terahertz bands cross-links in low Earth orbit satellite networks for 6G and beyond," *IEEE J. on Sel. Areas in Commun. (Early Access)*, Feb 2024.

[4] M. Giordani and M. Zorzi, "Non-terrestrial networks in the 6G era: Challenges and opportunities," *IEEE Network*, vol. 35, no. 2, pp. 244–251, Mar–Apr 2021.

[5] M. Sundarum, "Update on 5G non-terrestrial networks briefing paper," *5G Americas*, Jul. 2023.

[6] J. Fomon, "New speedtest data shows starlink users love their provider," May 2023. [Online]. Available: https://www.ookla.com/articles/starlink-hughesnet-viasat-performance-q1-2023

[7] H. Kaushal and G. Kaddoum, "Optical communication in space: Challenges and mitigation techniques," *IEEE Commun. Surveys & Tutorials*, vol. 19, no. 1, p. 57–96, Aug 2017.

[8] A. N. Kolmogorov, "The local structure of turbulence in incompressible viscous fluid for very large Reynolds numbers," *Soviet Physics Uspekhi*, vol. 10, no. 6, p. 734, Jun. 1968.

[9] L. C. Andrews and R. L. Phillips, *Laser beam propagation through random media*, 2nd ed. Bellingham, Wash: SPIE Press, 2005.

[10] R. Rui-Zhong, "Scintillation index of optical wave propagating in turbulent atmosphere," *Chinese Physics B*, vol. 18, no. 2, p. 581, Feb. 2009.

[11] A. Ashraf, A. Zaghloul, A. A. Shaalan, and H. Kasban, "Effect of fog and scintillation on performance of vertical free-space optical link from Earth to low Earth orbit satellite," vol. 39, p. 294–304, May–June 2021.

[12] S. Nie and I. F. Akyildiz, "Channel Modeling and Analysis of Inter-Small-Satellite Links in Terahertz Band Space Networks," *IEEE Trans. on Commun.*, vol. 69, no. 12, p. 8585–8599, Dec. 2021.

[13] T. S. Rappaport *et al.*, *Radio Propagation Measurements and Channel Modeling: Best Practices for Millimeter-Wave and Sub-Terahertz Frequencies*. Cambridge University Press, 2022.

[14] J. Kokkoniemi *et al.*, "Channel modeling and performance analysis of airplane-satellite terahertz band communications," *IEEE Trans. on Veh. Tech.*, vol. 70, no. 3, p. 2047–2061, Mar. 2021.

[15] V. Petrov, D. Moltchanov, and J. M. Jornet, "Accurate channel model for near field terahertz communications beyond 6G," in *2024 IEEE 25th International Workshop on Signal Processing Advances in Wireless Communications (SPAWC)*, September 2024, pp. 781–785.

[16] Yang, Zhirong and Gao, Weijun and Han, Chong, "A Universal Attenuation Model of Terahertz Wave in Space-Air-Ground Channel Medium," *IEEE Open Journal of the Communications Society*, vol. 5, pp. 2333–2342, 2024.

[17] J. Kokkoniemi, J. Lehtomäki, V. Petrov, D. Moltchanov, and M. Juntti, "Frequency domain penetration loss in the terahertz band," in *2016 Global Symposium on Millimeter Waves (GSMM) & ESA Workshop on Millimetre-Wave Technology and Applications*, June 2016, pp. 1–4.

[18] J. M. Jornet and I. F. Akyildiz, "Channel modeling and capacity analysis for electromagnetic wireless nanonetworks in the terahertz band," *IEEE Trans. on Wireless Commun.*, vol. 10, no. 10, p. 3211–3221, Oct. 2011.

[19] W. Gao, C. Han, and Z. Chen, "Attenuation and Loss of Spatial Coherence Modeling for Atmospheric Turbulence in Terahertz UAV MIMO Channels," *IEEE Transactions on Wireless Communications*, vol. 23, no. 9, pp. 11 636–11 648, 2024.

[20] J. C. Wyngaard, Y. Izumi, and S. A. Collins, "Behavior of the refractive-index-structure parameter near the ground∗," *J. Opt. Soc. Am.*, vol. 61, no. 12, pp. 1646–1650, Dec 1971. [Online]. Available: https://opg.optica.org/abstract.cfm?URI=josa-61-12-1646

[21] R. E. Hufnagel, "Propagation through atmospheric turbulence," in *The Infrared Handbook*, 1974, ch. 6, pp. 519–574.

[22] G. C. Valley, "Isoplanatic degradation of tilt correction and short-term imaging systems," *Applied Optics*, vol. 19, no. 4, p. 574–577, Feb. 1980.

[23] J. Federici and L. Moeller, "Review of terahertz and subterahertz wireless communications," *J. of A Physics*, vol. 107, no. 11, Jun. 2010.

[24] "The Atmosphere — National oceanic and atmospheric administration." [Online]. Available: https://www.noaa.gov/jetstream/atmosphere

[25] M. A. Al-Habash, L. C. Andrews, and R. Phillips, "Mathematical model for the irradiance probability density function of a laser beam propagating through turbulent media," *Optical Eng.*, vol. 40, no. 8, p. 1554, Aug. 2001.

[26] L. C. Andrews, R. L. Phillips, and C. Y. Young, "Scintillation model for a satellite communication link at large zenith angles," *Optical Eng.*, vol. 39, no. 12, p. 3272–3280, Dec. 2000.

[27] C. W. Higgins, M. Froidevaux, V. Simeonov, N. Vercauteren, C. Barry, and M. B. Parlange, "The effect of scale on the applicability of Taylor's frozen turbulence hypothesis in the atmospheric boundary layer," *Boundary-Layer Meteorology*, vol. 143, no. 2, p. 379–391, May 2012.